Journal of Ocean Engineering and Science 7 (2022) 41–57

Contents lists available at ScienceDirect

Journal of Ocean Engineering and Science

journal homepage: www.elsevier.com/locate/joes

Dynamic evaluation of jack-up platform structure under wave, wind, earthquake and tsunami loads

Zaid Mohammed Ghazi[a], Imad Shakir Abbood[a,b,*], Farzad Hejazi[a]

[a] Department of Civil Engineering, Universiti Putra Malaysia, Malaysia
[b] Engineering Affairs Department, Sunni Endowment Diwan, Baghdad, Iraq

ARTICLE INFO

Article history:
Received 25 June 2020
Revised 9 April 2021
Accepted 27 April 2021
Available online 8 May 2021

Keywords:
Offshore structures
Earthquake
Dynamic excitation
Jack-up platform
Tsunami
Seismic zone

ABSTRACT

Nowadays, the demand for using jack-up platforms to carry out a large percentage of deep-water oil and gas exploration is steadily increasing. The response of jack-up platforms to the severe dynamic loads that may be encountered during the structure life is not examined enough. Therefore, this study attempts to investigate the response of jack-up platforms performance under the effect of dynamic loads due to wave, wind, earthquake and tsunami forces using the finite element method for two models with the lowest and highest hull elevations. The jack-up platform is located in the Gulf of Mexico. Earthquake accelerations are applied to the model in high and moderate seismic levels. In addition, tsunami waves are applied to the platform in three different directions at 0°, 45° and 90°. This study utilised Airy's linear wave approach to assess the surface elevations and wave kinematics. The reference wind velocity is 10 knots at 10 m over the mean water level. Results indicate that the dynamic response of the structure is affected by the height of the platform and by the increase of the platform hull elevation. The combination of the El-Centro earthquake, dead and live loads provides the major impact on the platform at the lowest (70 m) and highest (85 m) hull elevations. The comparison of all result proves that the jack-up platform hull under high earthquake intensity and tsunami waves with 45° has experienced maximum deformation. Moreover, raising the deck will increase the response of the dynamic load and displacements but will negatively affect the platform.

1. Introduction

Offshore oil and gas investigation began in the early 19th century. Nowadays, wide varieties of these structures are being used despite their existing challenges in extreme environmental conditions [1,2]. Although the reinforced concrete structure has accurate durability [3,4], most of the jack-up platform is made of steel because of its durability, long life and tension resistant to the steel structure. Jack-up platforms have several tubular legs, which could be moved up and down through cut-outs in the pontoon. A jack-up rig is one of the mobile platforms that consist of a buoyant hull fitted with movable legs [5]. We regarded these platforms as "jack-up" because they are self-elevated units with three or four movable legs that can be jacked through the hull. Approximately 53% of the failures experienced by jack-up platforms are caused by the punching through their legs. The starting point for all offshore structural analysis is the estimation of the forces generated from fluid loading [6,7]. In shallow water, the critical wave height exponent has been shown to vary significantly with structural configuration [8-10]. Critical wave height exponent is also sensitive to the wave theory chosen because of the strong relationship of wave kinematics. In shallow waters, accurate modelling of large waves is more challenging compared with deep water due to higher relative wave height [11].

The American Petroleum Institute (API) posits that the wave crest height is higher than the lower deck elevations of many existing platforms [12,13]. The API guideline also indicates that most platforms cannot survive wave forces acting on the decks. A new systematic integrated information modelling based on virtual prototyping of the jacking system has been considered. The realisation of the driving function is given as an example of a jacking system, which demonstrates that the methodology is noticeably helpful for integrated information modelling [14].

The decks must be raised to clarify the specified wave crests according to the calculated crest of the design wave with an adequate allowance of safety [15]. However, with the occurrence of

* Corresponding author.
E-mail address: imadshakirabbood@gmail.com (I.S. Abbood).

https://doi.org/10.1016/j.joes.2021.04.005

a tropical storm or hurricane, the wave height exceeds the design height. A five-feet safety air gap should be added to the crest elevation to water depth to avoid waves striking the deck. The platform deck rises to determine the minimum acceptable elevation of the bottom beam of the lowest deck for the possibility of extreme waves [12]. One of the air gap problems is the water on the deck, or slamming to the hull during extreme waves may damage the floating offshore structure [16]. The crest amplitude of the waves is the most important aspect to measure air gap height.

The major effect of an earthquake that designers concerned about are the failure at joints, cracking in walls and foundation, bridge deck displacement, ruptures in pipelines and soil liquefaction and the hull substructures collapse. During the last few years in Malaysia, seismic risk has caused growing concern. Although the seismic risk is very small in comparison to countries such as Japan and Indonesia, this risk should not be completely ignored.

The disaster of a tsunami prompted considerable re-thinking amongst the coastal engineering community [17], which has now started to classify tsunami events according to their level of severity and intensity into two different levels [2,18,19]. For the first level of tsunami, events would have a return period of more than 100 years, which is relatively low in height. From another perspective, the second level of tsunami events takes a few hundreds of years. Inundation heights for the event in Level 2 would be much higher, typically over 10 m but would encompass up to 30 m in height in some events [20]. The primary reason for this distinction is the unique timescale associated with tsunami phenomena. Tsunami wave periods range from a few minutes to over 1 hour unlike typical water waves generated by the wind with periods between 5 and 20 second [21].

In particular, offshore structure footings have finite stiffness in horizontal, vertical and rotational directions, cross-coupling exists between the horizontal and rotational degrees of freedom and nonlinearity may occur [22,23]. The simplest type of soil-structure interaction is assuming that the foundation can be modelled as a fixed joint [24], which is a 100% fixity condition. Chaudhry [25] discussed the effect of foundation fixity of jack-up units under extreme loading conditions. The frequency of operational accidents for jack-up structures is much higher than that of fixed offshore platforms. The accident statistics for fixed offshore structures have improved with time, whereas jack-up platforms accidents have worsened with the increasing use of water [6].

Most of the studies focused on the effect of the jack-up platform structures under ocean waves, earthquake or tsunami only. Thus, additional research is needed to evaluate the effect of the same jack-up under those loads in addition to the wind load. Therefore, this study aims to identify the dynamic response of jack-up structures and their sub-structures, with two different platform hull elevations, under various load combinations in a lower and higher level of the platform.

2. Significance of research

Inadequate knowledge of the situation and deficiency of evolution is usually the main cause of any structural collapse [26]. To avoid unnecessary risk after installing and facing environmental loads, changing the analysis techniques must be considered. Based on the need for a more extended duty of jack-up platforms in each situation, including their application in deeper water and crucial circumstances, long-term reliability investigates the response of jack-ups during a dangerous difficult situation [27,28]. Wind loads are not usually considered as a key factor in the total loading of ships and offshore platforms [29]. Given the size of the common static loads and the moments produced by the wind, critical cracks and obstructing efficiency during offshore operations will induce. The wind load (induced form drag force) is represented as the cumulative loads incorporated with linear and non-linear expressions of wind speed [30]. Thus, the wind loads must be taken into account in the calculation to provide a more powerful design with the equivalent size [31,32]. When an earthquake combines with other loads, such as tsunami, winds and/or waves, the resultant of displacements will be greater than the displacement response of earthquake load alone [33].

Fig. 1. Bethlehem JU 250 MS, jack-up offshore structure in the Gulf of Mexico (www.offshoreenergytoday.com).

Load combinations primary influence the durability, life and dynamic properties of the platforms, which leads to the vibrations of platforms, damage and malfunction of platform equipment [34]. Thus, the load combinations were applied in this research on the same structure with different deck elevations to assess the response of jack-up platforms under the highest and the lowest hull elevation. The jack-up platform structure is located in the Gulf of Mexico. Wave and wind forces were implemented on the fixed ground platform structure in addition to the alive and dead loads. Airy's linear wave theory was used to define ocean wave characteristics. The El-Centro and Malaysian seismic zones were implemented also under high and moderate earthquakes. Tsunami waves were applied in three different directions at 0°, 45° and 90°

3. Jack-up platform

This study used the Bethlehem JU 250 MS, the jack-up self-elevating drilling structure with three columnar legs located in the Gulf of Mexico, as shown in Fig. 1. The platform hull overall length is 50.5 m, width is 40 m and its depth is 4.8 m. The forward leg spacing is 33 m and between the port and starboard 31.5 m. The Bethlehem hydraulic jacking system is used to elevate the hug mass of the deck hull and its sub-structures. The three legs are made of steel (A678 grade B) with 95 m length each with a mat foundation. The mean water depth was assumed to be 60 m with a maximum water height of 75 m. The slot drilling rig is outfitted for 6-km drilling.

The hull was assumed as a beam component with corresponding stiffness and masses held by the rigid leg-hull connection. Non-linearity in the leg-hull jack was significantly recognised although they were not involved in the analyses. The hydrodynamic modelling of the leg was conducted by idealising the complete frame leg to comprise one "equivalent" perpendicular tubular segment located at the geometric centroid of the actual leg.

The jack-up platform was modelled and analysed through a finite element program (SAP2000). Fig. 2 shows the modelling of the jack-up platform was conducted with the lowest and highest

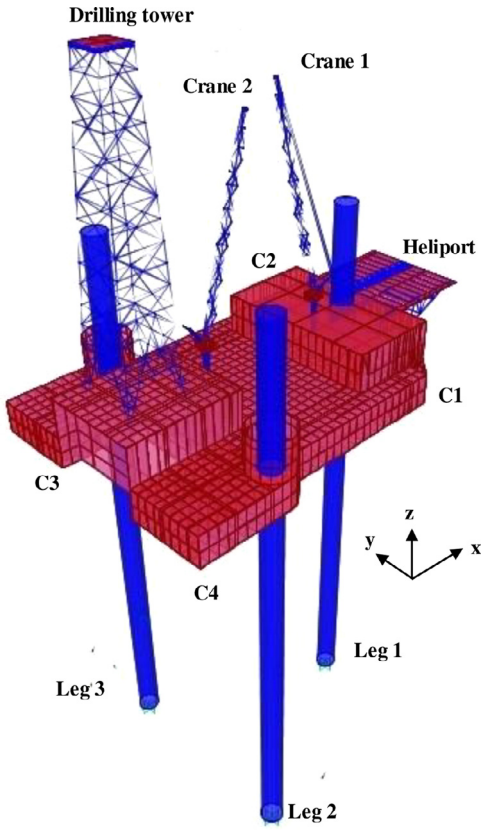

Fig. 2. Modelling of jack-up platform.

hull elevations with the three-column legs (1, 2 and 3). In addition, three sub-structures include drilling tower, heliport and two cranes and four hull corners (C1, C2, C3 and C4). The estimation of the forces generated by the environment or by the machines on the deck was the starting point for jack-up platforms. Structural loads are applied to the structure according to the drawing layout. The analysis of the structure was the assessment of the load combinations by using SAP2000 according to code criteria [12].

4. Structural loads

4.1. Dead loads

All the permanent parts in the platform deck represent the dead loads. The platform was built for multipurpose, such as drilling, wellhead type platform or process type platform, which maintains different devices and equipment. Dependant structural objects, such as boat landing, handrails, deck plating and small access platforms, were attached to the platform weight. The weight of the platform hull with all the drilling equipment and other facilities is approximately 15,000 tons. From another perspective, each tubular column weight is approximately 800 tons, which was made of high strength steel. Fixed items and non-structural components have no stiffness to contribute to the global integrity of the platform and should not be modelled. The permanent load of the machinery and other equipment dead load are applied as a distributed load of 8.75 kN/m² on the surface of the platform. When computer software was used to analyse the model, primary steel structural members were considered according to the structural information. Furthermore, the weight of dependant steel structural parts was calculated and applied to the model at suitable places according to the structural plan.

Table 1
Live loads.

Location	Load (kN/m²)
Storage	10
Walkway	5
Access platform	5
Galley	10

4.2. Live loads

The live load was applied to the designated areas as a distributed load (3 kN/m²) in the living quarters and drilling area. Other live loads including open areas were applied as shown in Table 1. The loading and unloading areas carry 5 kN/m². These loads should be applied as deemed necessary by the administrator of the platform.

4.3. Lateral loads

Offshore facilities are located in the ocean for the discovery, and the development of resources is always under multiple load types, particularly the wind loads, which control the characteristics of the ocean waves. All actions should be ended, and tools and buildings should be protected when the storms defeat the design system. Winds, waves, tsunamis and earthquakes are the most environment loads that may be faced by the structures.

4.3.1. Waves and wind loads

Generally, sea states are multidirectional and random in nature. For deep waters or where platforms tend to be more flexible, the static analysis may not be able to adequately describe the true dynamic loads. The wave theories are extremely valuable for offshore constructions and their fundamental segments. The computation of the wave kinematics, such as velocity and acceleration, involve the equations from wave theory. Various kinds of solutions are available depending on the accuracy required and the parameters involved in the computation. Depending on the location, deep or shallow water and associated wave parameters, a suitable wave theory was selected for use [12,35]. The wave loads (gravity waves) used for the jack-up was exerted sideways on the main columns and produces moment resistant on the fabrication. Most of the wave energy is released by the gravity waves. During the design of offshore structures, the highest wave should be utilised. The significant wave height (H_s) and maximum wave height (H_{max}) are presented in Eq. (1) as follow:

$$H_{\max} = 1.86 \times H_s \tag{1}$$

Airy's linear wave theory was selected to assess surface altitudes and wave kinematics because this theory was the simplest and the most applicable linear wave theory. Waves create a free surface movement at the mean water surface performed simultaneously by gravity. The altitude of the free surface alters with time and space. Airy's linear wave was determined by giving the wave elevation time and type designated as Airy's wave in the finite element method options. In Eq. (2), Airy's wave has a sine curve form and free surface profile, which could be written simply in the following form:

$$\delta = \mathrm{A} \times \sin(\mathrm{kx} - \omega t) \tag{2}$$

where δ, *A, kx and wt.* represent the displacement (mm), amplitude (mm), wave-number and angular-frequency (rad/s) respectively. Conventional waves have the properties of holding a time such that every sequence owns the same model. Consequently, the theories describe the characteristics of one period of the conventional waves and these characteristics are constant from period to

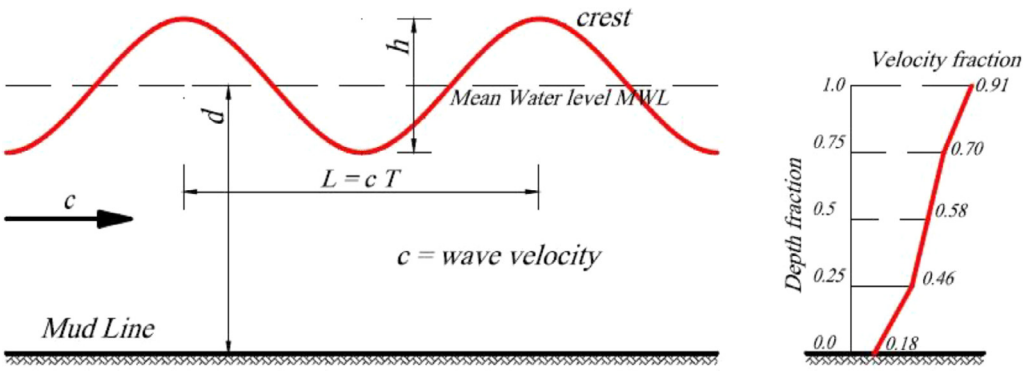

Fig. 3. Wave coordinate system with typical wind and tidal current profile [11].

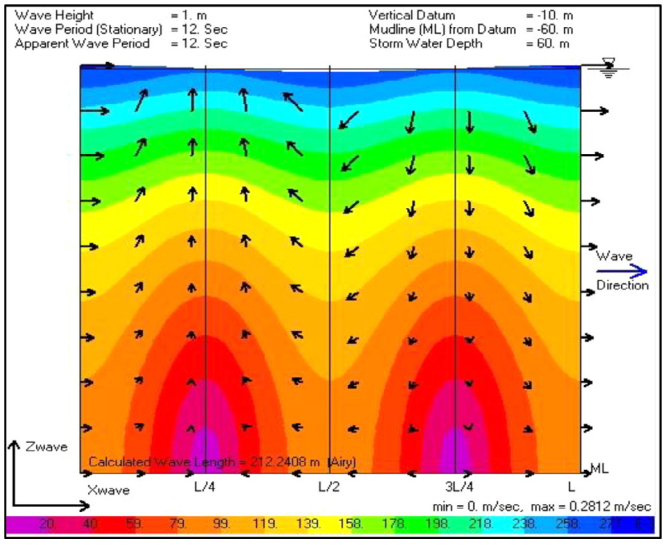

Fig. 4. Water properties.

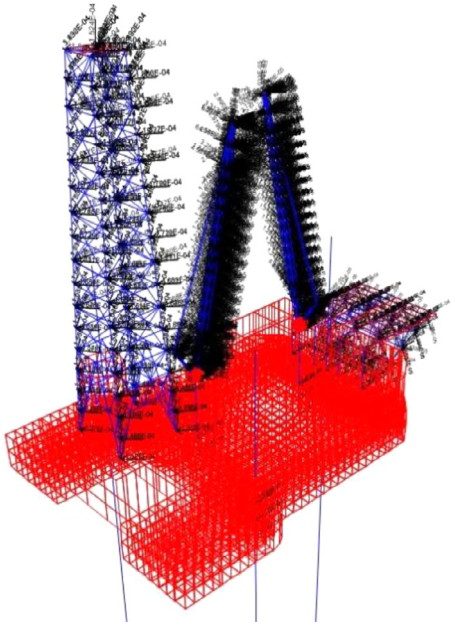

Fig. 5. Distribution of wind loads.

period. Fig. 3 shows the three factors required in expressing each wave theory [11], namely, time period (T), height (H), and water depth (d). For wave theories, the floor was assumed to be horizontal and flat.

Wave load was defined in SAP2000 by providing the linear wave theory, wave height, wave period and some other parameters. Airy's wave was demonstrated by providing the wave height of 1 m in 60 m of water depth and 12 s of wave period. The maximum wave speed of 0.2812 m/sec and the vertical datum of 10 m was the air gap between the lower deck and the water level (Fig. 4).

In offshore structures, wind forces are usually small compared with the hydrodynamic forces. They account for about 15% of the total environmental loading on a structure under extreme conditions, and less than 10% in a minor contribution in relatively shallow waters [12]. The forces should not be ignored. However, they can affect the overturning moment because the long lever arms developed as the water depth increases. In deeper water and for compliant designs, wind loads can be significant and must be studied in detail.

To proceed with wind loading calculations, a reference wind velocity associated with the return period for the site must first be specified. These reference velocities are specified at normally 10 m (in offshore industry) above the mean water level. The wind direction and speed vary in space and time. The cumulative wind load (drag force) on the platform can be determined by Eq. (3):

$$F = \left(\frac{\rho}{2}\right) \times U^2 \times C_s \times A \tag{3}$$

where F, ρ, U, C_s and A represent the force (N), the mass density of air (1226 kg.m^3), 1-minute mean wind speed (m/s), shield factor (1), and wind surface (m^2), respectively. The wind load value was normally inputted directly at the relevant nodes in numerical analysis procedures [36]. The wind velocity was 10 knots, and the shielding factor was approximately 0.85. Wind loads can easily and accurately be applied for any specific region when using SAP2000. This platform is located in a wind field. Fig. 5 shows the wind characteristic and how it is applied to the structure.

4.3.2. Earthquake excitation

Designing an offshore structure to resist severe earthquake ground shaking is uneconomical but is necessary for fixed offshore structures. For design and analysis purposes, the time variation of ground acceleration is the most useful way to define ground shaking during an earthquake. In preliminary consideration, an evaluation of seismic activities is necessary for the offshore structure design.

The El-Centro and Malaysian seismic zone were implemented as earthquake excitations in high and moderate earthquake levels. The El-Centro earthquake was applied in three different directions,

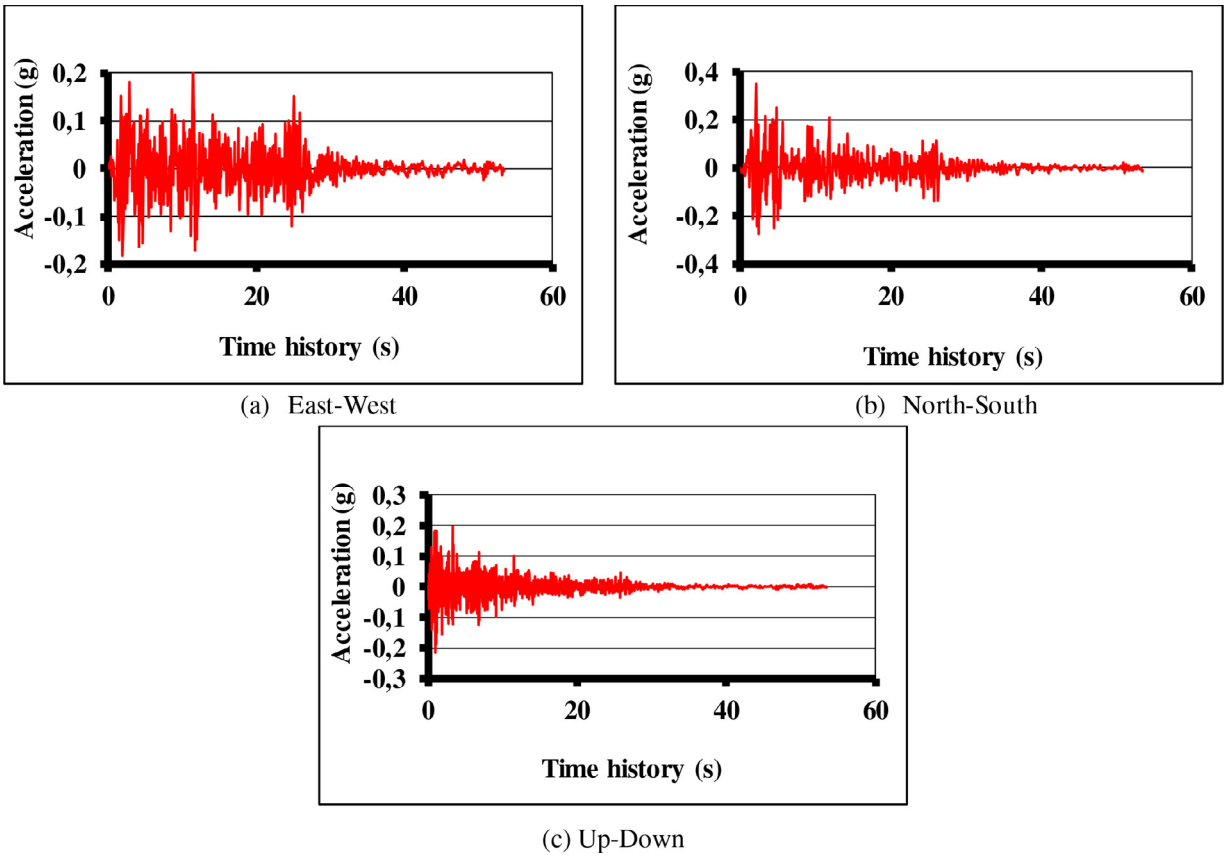

Fig. 6. El-Centro earthquake wave in three different directions.

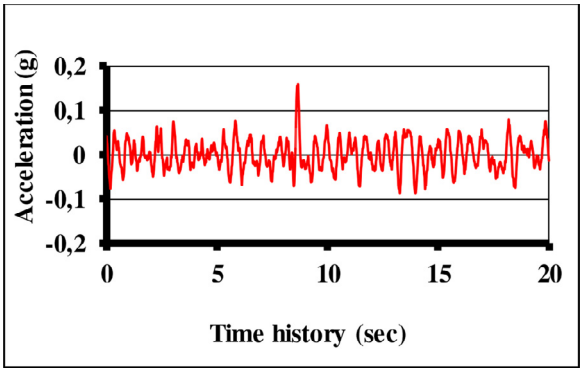

Fig. 7. Malaysian earthquake wave in one direction.

that is, north-south, east-west and up-down, as shown in Fig. 6. The number of output steps is 2674 with a time of 0.02 s for each step.

Malaysian earthquake was applied to the structure for just one direction (U1) as shown in Fig. 7. The number of output steps was 1000 with a time of 0.02 s for each step. The analysis of the structure under the earthquake effect was done by using SAP2000 according to API criteria.

4.3.3. Tsunami wave

In deep water, ocean tsunami waves have extremely long wavelengths. Tsunamis cause much further damage than regular waves do due to the large water mass that can proceed to speed for an elongated duration. Models of fluid motion calculate individual fluid particles. Tsunami height and speed vary in space and time.

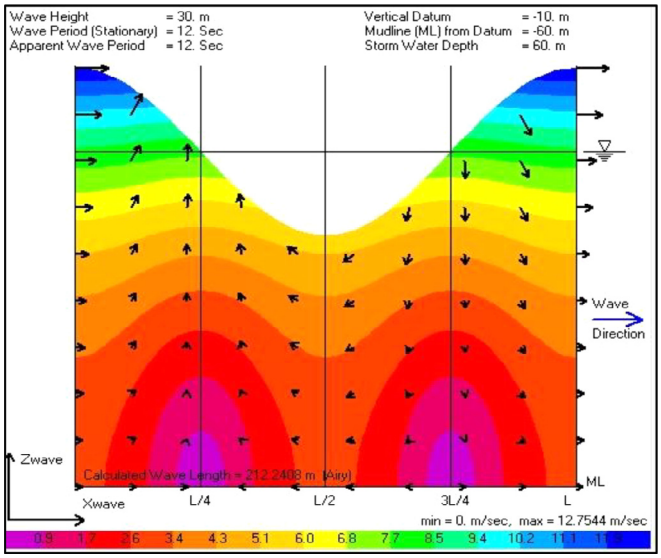

Fig. 8. Tsunami water properties.

The speed of tsunami can be calculated in Eq. (4) as follows:

$$Speed = 3.13\sqrt{h} \tag{4}$$

where h is the depth of the ocean. Eq. (5) shows the formula of tsunami wave pressure calculation.

$$Q_z = \rho \times g \times (a_h - z) \tag{5}$$

where

Q_z: tsunami pressure (kN)

ρ: the unit volume mass of water, 1.0 (t/m^3)

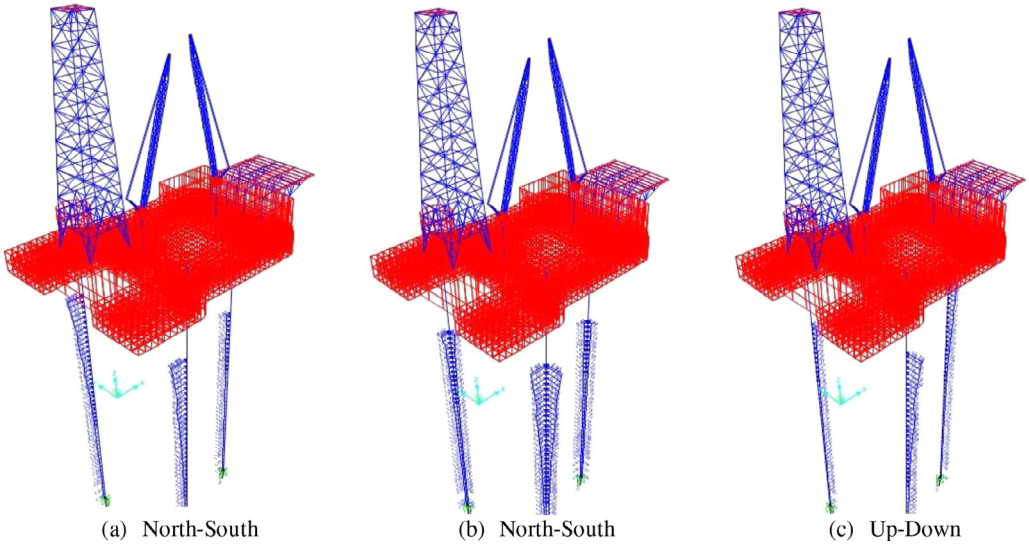

Fig. 9. Tsunami waves in three directions.

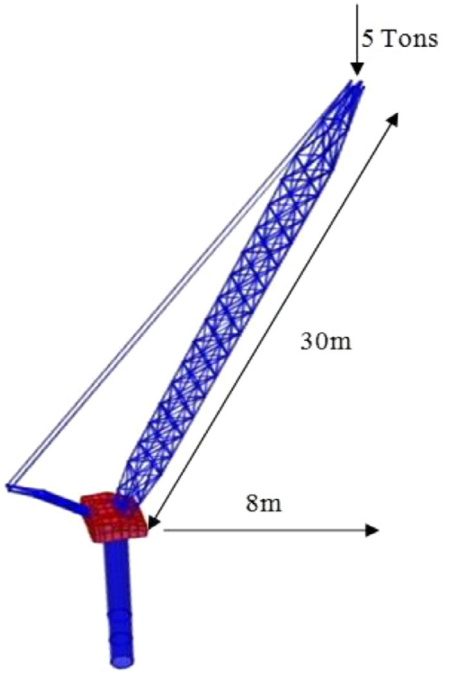

Fig. 10. Crane model.

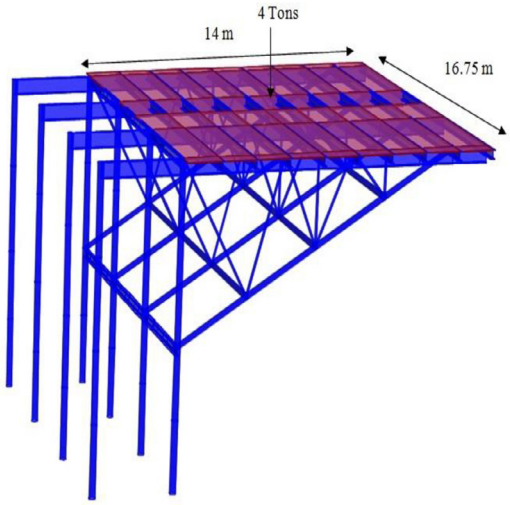

Fig. 11. Helicopter port model.

g: gravitational acceleration, 9.8 (m/s^2)

a_h: inundation depth for designing (m)

z: the height of the regarding part from the ground level ($0 \leq z \leq a_h$) (m)

a: Water depth factor (an offshore structure without shelter equal to 3).

The acceleration, velocity, position and mass were utilised as a description modelling the forces and dynamics of the tsunami particles. This modelling would help potentially to constrain dangerous situations and casualties. Tsunami waves in three different directions were carried out on the same platform structure with the highest and lowest hull elevations for the same water properties. Fig. 8 shows the tsunami wave direction with a maximum speed of 12.7544 m/sec and a wave height of 30 m.

Three different directions of tsunami waves were applied at 0°, 45°, and 90° (Figs. 9). To assess the effect of applying tsunami wave in different directions, sections, geometry members and materials properties of the structure are considered to be the same. Horizontal and vertical displacements for load combinations in two different levels of the main hull are compared. Then, the analysis of the structure under tsunami wave is done by using SAP2000 under API criteria.

5. Sub-structure modelling of the jack-up platform

One of the basic objectives of this research is to evaluate the main hull of the platform structure under dynamic loads. Nonetheless, studying the hull effects only is not sufficient for the examination. Accordingly, some sub-structures need to be considered in this study.

5.1. Crane modelling

Offshore crane vessels are used to lift heavy loads on the deck or transfer equipment from ships to the platform deck. Crane is one of the superstructures, which should be considered during dynamic loads. Two cranes with a 30 m lever arm with a rating at 8 m radius built of the steel pipes (P2) section are utilised to lift 5 tons. The lever arm and the crane cabin are supported by a tubular

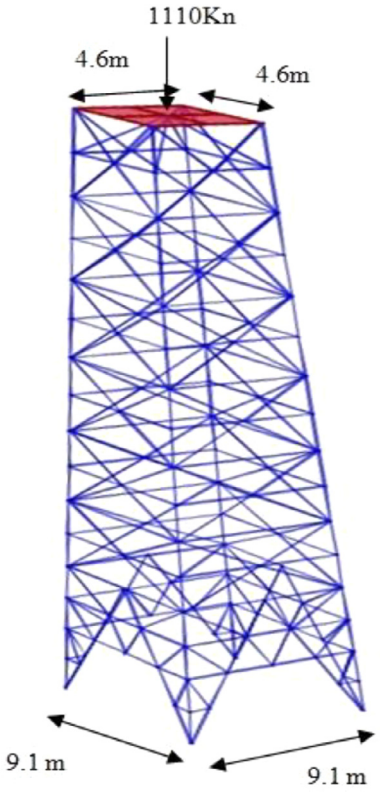

Fig. 12. Drilling tower model.

column of 0.9 m outer diameter fixed on the main hull, as shown in Fig. 10.

5.2. Helicopter port modelling

The landing helicopter on the heliport is considered an impact load. Then, the landing region for a helicopter is called the heliport. Manipulating the dynamic loads is sufficient and cost-saving (Fig. 11). The heliport has a side portion of 1.5 to 2 times the biggest helicopter's proposed length. The surface of the heliport must be created to control the concentrated force of 75% of the total weight. Furthermore, the impact load for a landing helicopter is approximately two times the total weight of the helicopter.

The helicopter port is one of the superstructures, which must be evaluated under helicopter loads and its impact during dynamic loads. The helipad is a cantilever port forward of living quarters (16.75 m x 14 m) to handle the load of landing and taking off of the helicopters. To support the port and the helicopter weight, a truss of steel pipes is connected to the main deck by eight columns, as shown in Fig. 11. This port can handle a helicopter with 4 tons of self-weight and two times this load as an impact load during landing and taking off.

5.3. Drilling tower modelling

The drilling tower is a long tower to support the drilling machine to drill wells up to (6 km) under the subsea (Fig. 12). Drilling loads are caused by drill rigs, which are large equipment assembled for drilling objectives and located on the head of the platform. The drilling rigs stiffness was not counted during fundamental designs, but the drilling rig mass was utilised as a load on the platform. Therefore, additional loads throughout drilling were settled due to drilling sequence and dragging progress. The drilling tower was built of (L4×4 × 1/2) steel sections. The tower bottom area is 9.1 m x 9.1 m and the top area is 4.6 m x 4.6 m, with a total height of 43.5 m. During the load (1110 kN) of the drilling machine and its vibration, the tower may be affected.

6. Results, findings and discussions

The analysis results for the combination of different loads were investigated. The horizontal and vertical displacements (Δ) in two different levels (70 and 85 m) of the main hull were compared as well. All segments' strength analyses were conducted according to the specifications of API. In addition, the structure collapsed to cross the API approval standards.

6.1. Hull displacements in 70 and 85 m elevation

6.1.1. Causes of normal wave and wind loads

Horizontal and vertical displacements within the lowest and highest hull elevations for the columns and some sub-structures were compared. Table 2 shows that the four corners of the main hull are moving simultaneously, but the displacement is getting higher when the hull is at 85 m elevation. The two cranes had the highest displacement in all directions. The reason for having maximum displacements of 733 mm in crane 1 and 580 mm in crane 2 was because of the long arm of the crane, the high amount of loads and the low stiffness of the crane. On the other hand, the horizontal movements of the heliport within the two different elevations of the main hull were moved with the platform movement. The vertical displacement of the heliport which was much important to consider was approximately 30 mm at the highest level of the hull and approximately 25 mm at the lowest level. The increment of the vertical displacements of the heliport is approximately 15.5% when the main hull elevated from 70 to 85 m. Furthermore, the highest Δ_X and Δ_Y in the top end of the drilling tower was slightly higher than the displacement in the main hull because of the drilling tower height. The vertical displacement of 69.5 mm at the lower level of the hull was slightly increased to 72.6 mm at the highest level, with an increment of 4.25%.

Table 2
Horizontal and vertical displacements of sub-structures at 70 and 85 m under wave and wind loads.

Sub-structures	70 m hull elevation			85 m hull elevation		
	X (mm)	Y (mm)	Z (mm)	X (mm)	Y (mm)	Z (mm)
C1	4.2	0.4	21.4	5.44	0.56	24.9
C2	4.2	0.4	21	5.5	0.55	24.45
C3	4.2	0.36	17.9	5.5	0.52	20.9
C4	4.2	0.36	18.34	5.44	0.52	21.46
Crane 1	15.1	733.2	216	17	733	219.2
Crane 2	580	0.87	173	581.1	1.1	176.2
Heliport	5	0.5	25.2	6.6	0.7	29.8
Drilling tower	6.4	1	69.5	8.1	1.2	72.6

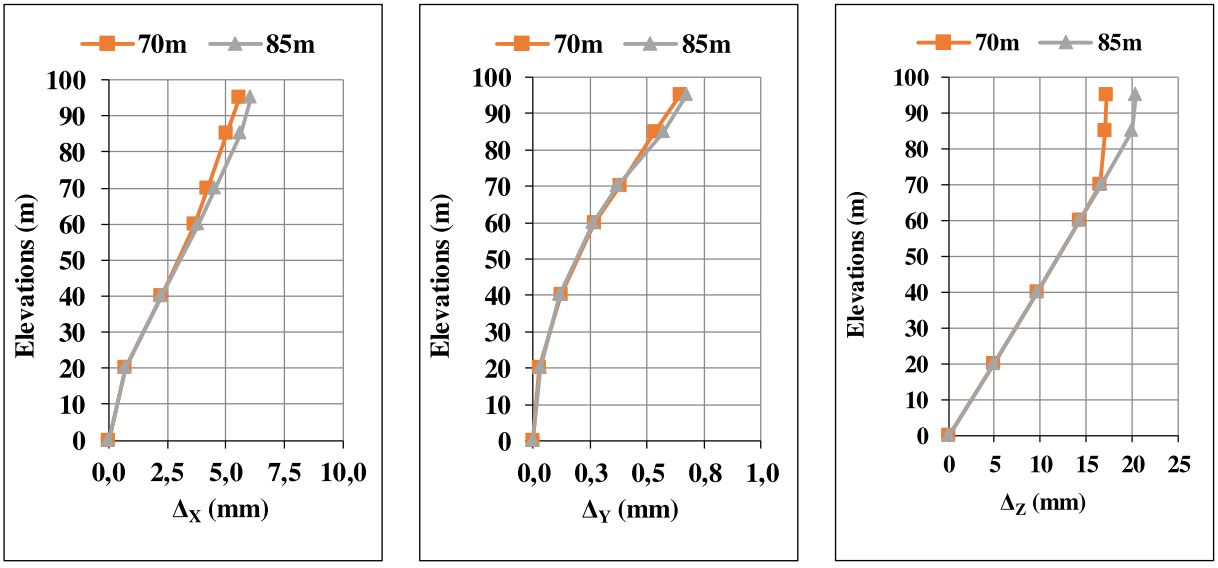

Fig. 13. Comparison of the two hull elevations vs. displacement under the normal wave and wind loads.

Table 3
Horizontal and vertical displacements of sub-structures at 70 and 85 m during El-Centro earthquake.

Sub-structures	70 m hull elevation			85 m hull elevation		
	X (mm)	Y (mm)	Z (mm)	X (mm)	Y (mm)	Z (mm)
C1	249.2	481	29.8	201.2	580	31.6
C2	226.7	481	30.8	201.4	579	31.2
C3	224	460	27.2	202	542.7	28.7
C4	252	460	28.5	202.7	542.7	28.6
Crane 1	306	1405	269	242.4	1428.5	255.1
Crane 2	867	610	188	801	657.8	182.2
Heliport	241	493	32.4	201.5	597	33.5
Drilling tower	256	498	72.3	211.6	576	74.6

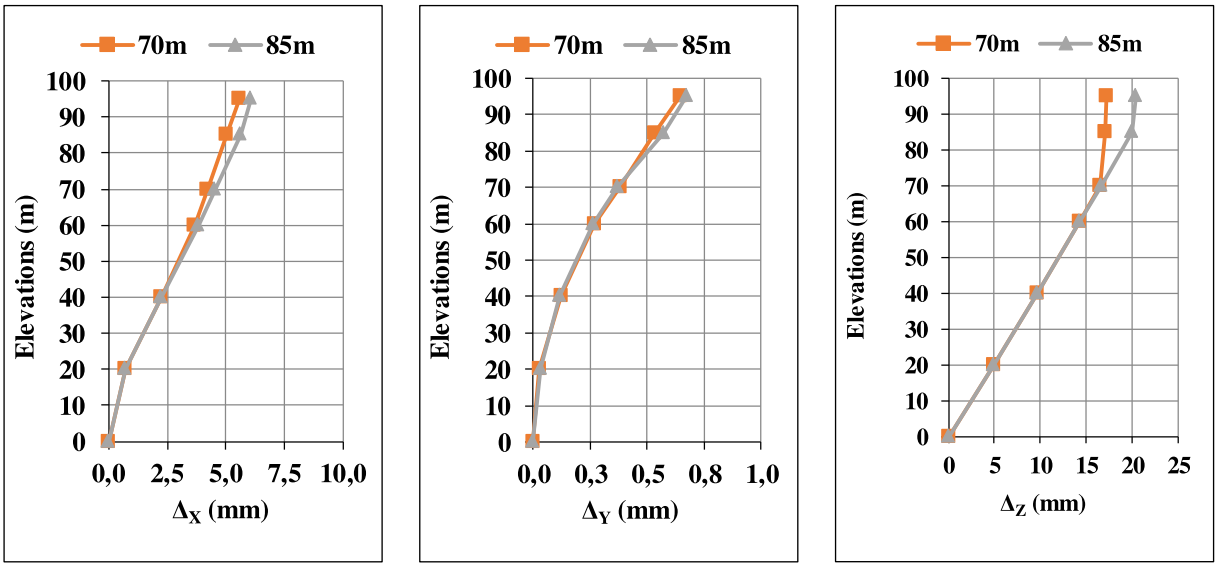

Fig. 14. Two hull elevations vs. displacement. under El-Centro earthquake.

Table 4
Horizontal and vertical displacements of sub-structures at 70 and 85 m during Malaysian earthquake.

Sub-structures	70 m hull elevation			85 m hull elevation		
	X (mm)	Y (mm)	Z (mm)	X (mm)	Y (mm)	Z (mm)
C1	49	0.8	22	58	0.8	25.5
C2	49	0.8	21.7	58	0.8	25.2
C3	49	0.91	18.9	58.3	0.85	21.5
C4	49	0.9	19.3	58.2	0.85	22
Crane 1	69	732	223	78	733	220
Crane 2	630	0.9	180.3	641	1.2	178
Heliport	48.8	1.3	26.9	59.4	1.2	30.5
Drilling tower	51.7	1.4	70.2	63.6	1.5	73

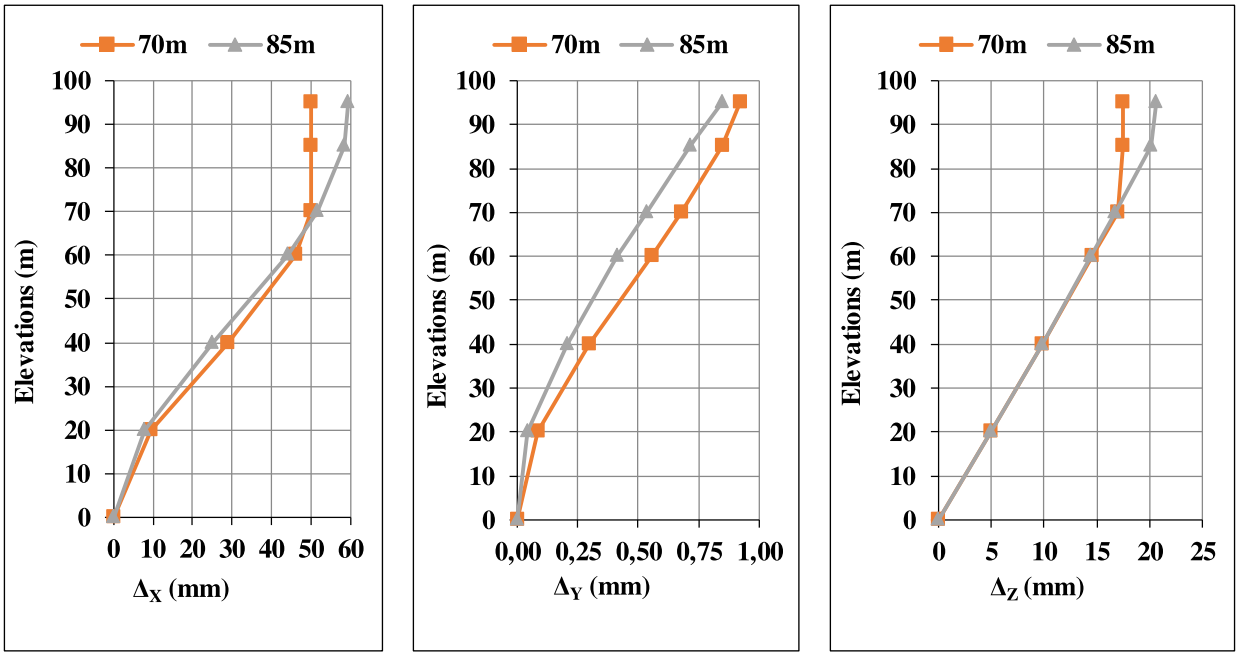

(a) X-direction (b) Y-direction (c) Z-direction

Fig. 15. Hull elevations at (70 and 80 m) vs displacement under Malaysian earthquake.

Table 5
Horizontal and vertical displacements of sub-structures at 70 and 85 m due to tsunami at 0°

Sub-structures	70 m hull elevation			85 m hull elevation		
	X (mm)	Y (mm)	Z (mm)	X (mm)	Y (mm)	Z (mm)
C1	206.8	0.44	23.5	297	0.65	27.1
C2	207	0.44	23.2	297	0.65	26.7
C3	207	0.3	15.2	297	0.46	18.2
C4	206.8	0.3	15.7	297	0.46	18.8
Crane 1	453.3	733.7	215.7	544	733	219
Crane 2	962	0.9	219.6	1053	1.2	223
Heliport	209	0.6	29.8	299	0.85	33.3
Drilling tower	233.1	0.92	67.6	323.6	1.1	70.8

Table 6
Horizontal and vertical displacements of sub-structures at 70 and 85 m due to tsunami at 45°

Sub-structures	70 m hull elevation			85 m hull elevation		
	X (mm)	Y (mm)	Z (mm)	X (mm)	Y (mm)	Z (mm)
C1	115.3	104	21.5	164.5	146.4	25.2
C2	113	104	23	161.2	146.4	26.7
C3	113	101	17.5	161	141	20.4
C4	115.6	101	15.8	164.8	141.7	18.9
Crane 1	358	840.3	215	406.8	882.2	219
Crane 2	866	104	225	917	146.2	222.8
Heliport	115	106	28	164.3	148.6	31.5
Drilling tower	137	103	68.5	187	144	71.6

Table 7
Horizontal and vertical displacement of sub-structures at 70 and 85 m due to tsunami at 90°

Sub-structures	70 m hull elevation			85 m hull elevation		
	X (mm)	Y (mm)	Z (mm)	X (mm)	Y (mm)	Z (mm)
C1	15.6	250	18.9	21.2	350.6	22.7
C2	9.2	250	23.8	17.3	350.6	27.2
C3	8.5	241	20.5	16.9	345.2	23.3
C4	16.2	241	15.3	21.6	345.2	18.4
Crane 1	253	989	218	261	1090	219.1
Crane 2	764	252	219	771.5	353.8	222.6
Heliport	13.2	255	26	20.1	354.2	29.7
Drilling tower	33.2	249	69.3	40.8	352.2	72.4

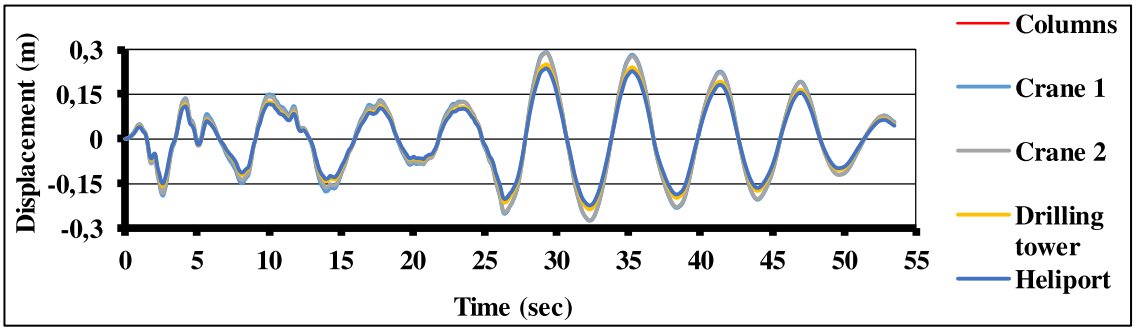

(a) X-direction

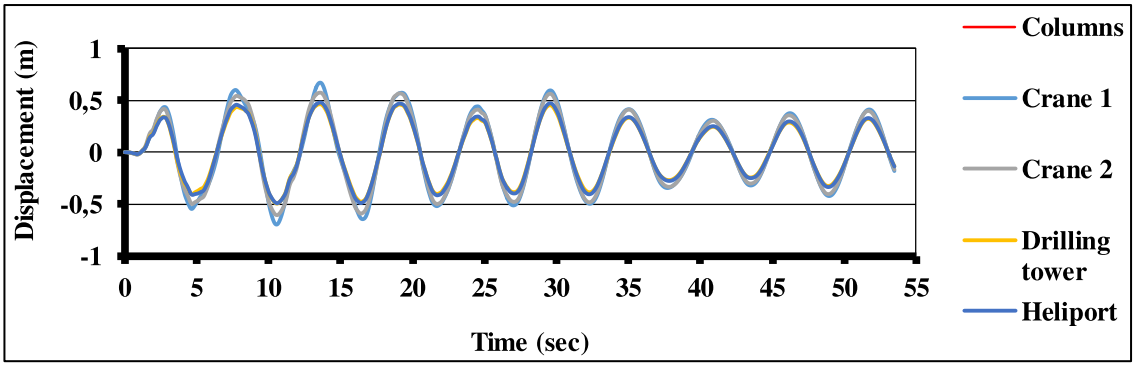

(b) Y-direction

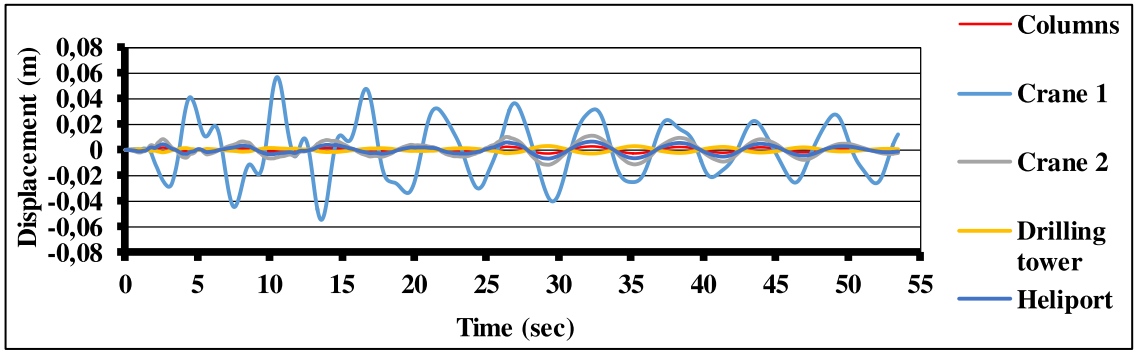

(c) Z-direction

Fig. 16. Displacements of columns and sub-structures during El-Centro earthquake at 70 m hull elevation in X, Y and Z directions.

The average displacements in each level of columns were calculated. Column displacements in each case were almost the same. Fig. 13 shows the comparison of the two hull elevations versus the displacement under the normal wave and wind loads. The three directions of the displacements when the hull was in the elevation of 85 m were greater than when the hull was at 70 m height. The Δ_X increased by 7.75% when the platform deck lifted from 70 to 85 m elevation. No much difference was observed in the Δ_Y in both models. Moreover, the average Δ_Z increased by 15.7% when the platform deck was higher. These differences in displacements mostly occurred at 70 m elevation and above. To conclude, the displacements become larger when the lever arm of the centre of gravity of the hull is longer.

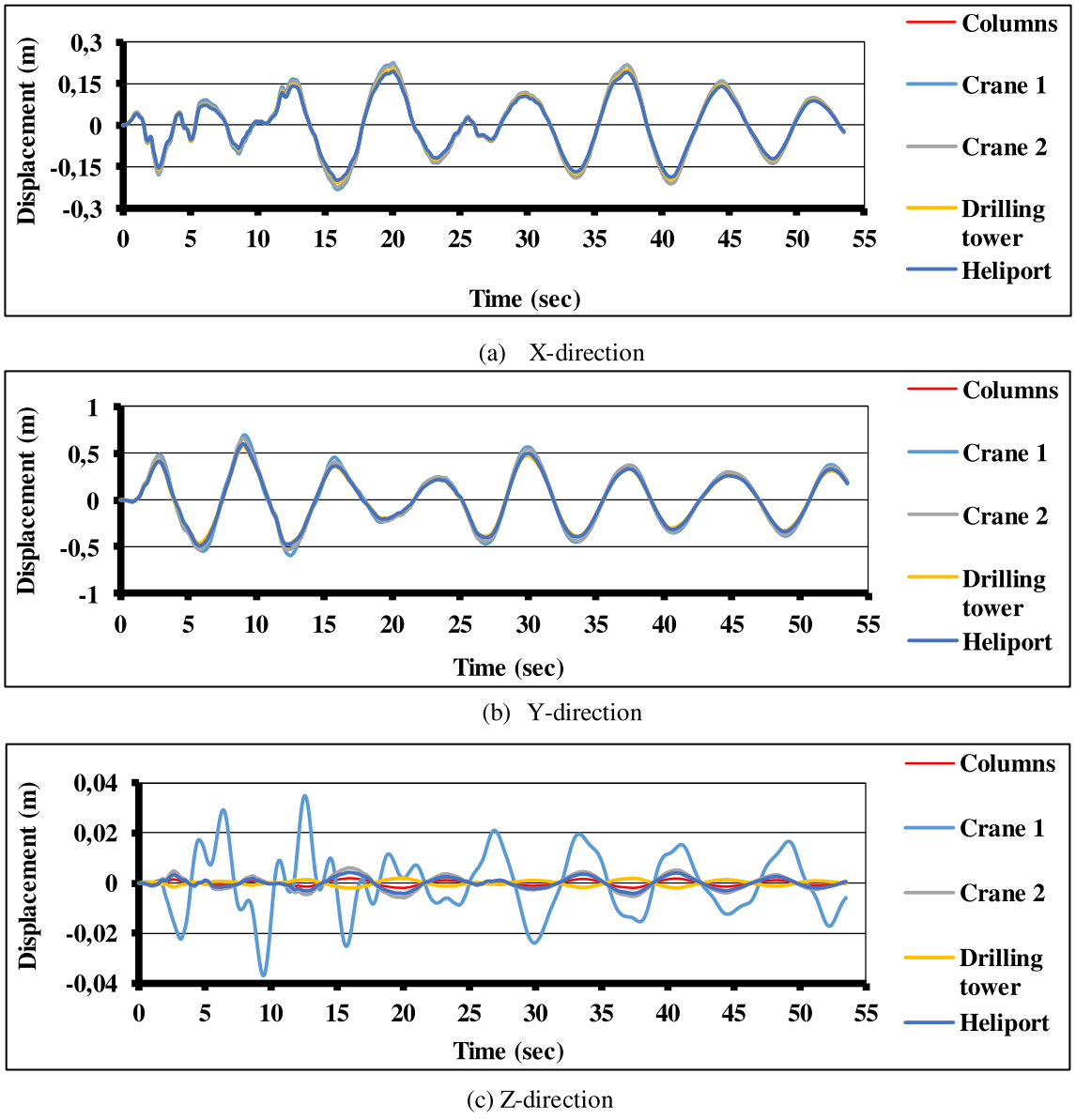

Fig. 17. Displacements of columns and sub-structures during El-Centro earthquake at 85 m hull elevation.

6.1.2. Causes of El-Centro earthquake excitation

Horizontal and vertical displacements during El-Centro earthquake recording for the two models were compared (Table 3). The displacements of the three columns in each model, four corners of the hull and the three substructures were also evaluated. Corners 1 and 2 of the hull have 21 mm in Δ_Y and Δ_Y greater than corners 3 and 4 when the hull is at 70 m elevation. When the platform deck is at 85 m elevations, the difference in Δ_Y for the same corners is approximately 37 mm. Thus, an approximately 43% difference exists in the displacement of the two models. The difference in the displacements between corners 1 and 2 and between corners 3 and 4 is approximately 22.5 mm and 28 mm, respectively. The hull seemed twisted, which would affect the serviceability of the main hull. By contrast, Δ_X for the four corners of the main hull elevation of 85 m was moved simultaneously whereas the maximum Δ_X for the 85 m hull elevation is 580 mm. When the hull is in 70 m elevations, the maximum Δ_Y is 481 mm, which is lower by approximately 17%. Furthermore, Δ_{Xs} are higher by approximately 16% when the hull was at the lowest level, and the difference in Δ_Z for the two models is approximately 3.4%.

Table 3 shows the vertical and horizontal displacements for the top of the two cranes, helicopter port and top of the drilling tower. Crane 1 has the highest displacement for the lowest and highest hull elevation of approximately 1405 and 1428.5 mm respectively with only a 1.65% difference. Crane 2 has high displacement in both vertical and horizontal directions, but they are quite similar in both models. The Δ_Z for the helicopter pad has been decreased by approximately 16.4% when the hull gets higher. Moreover, Δ_Y and Δ_Z for the heliport are increased by 17.4% and 3.3% respectively, when the platform deck rise. Eventually, Δ_X for the drilling tower decreased by 17.2% when the platform deck was at the highest level. On the contrary, Δ_Y and Δ_Z for the drilling tower increased by 13.5% and 3% respectively when the platform deck was lifted from 70 to 85 m. Table 3 also shows that all Δ_X for the corners and the sub-structures are decreased when the hull gets higher except crane 1. Moreover, Table 3 shows that Δ_Y and Δ_Z for the four corners and the sub-structures increased when the hull in the highest level except crane 1 also increased.

To compare these two cases of hull elevation under El-Centro excitation in terms of horizontal and vertical displacements, the

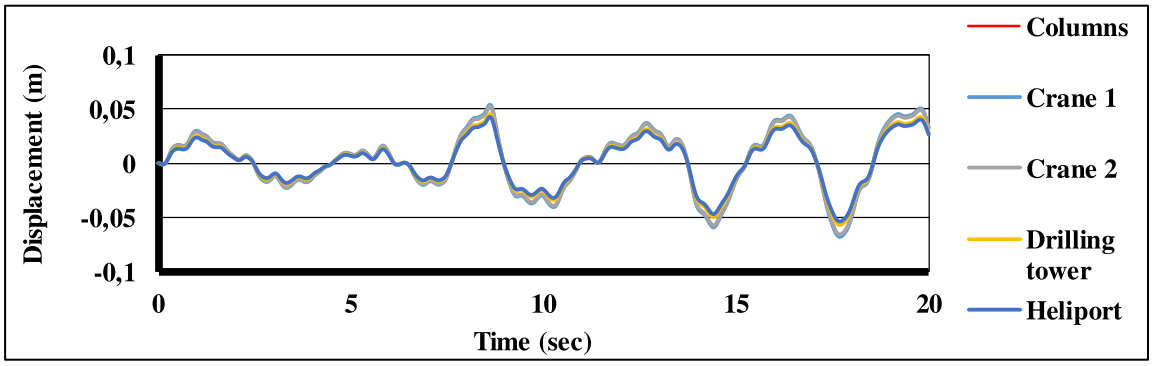

(a) X-direction

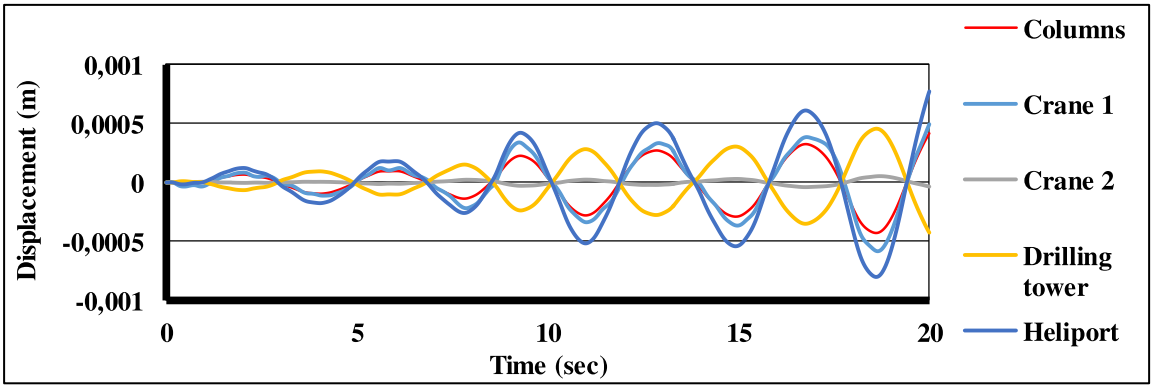

(b) Y-direction

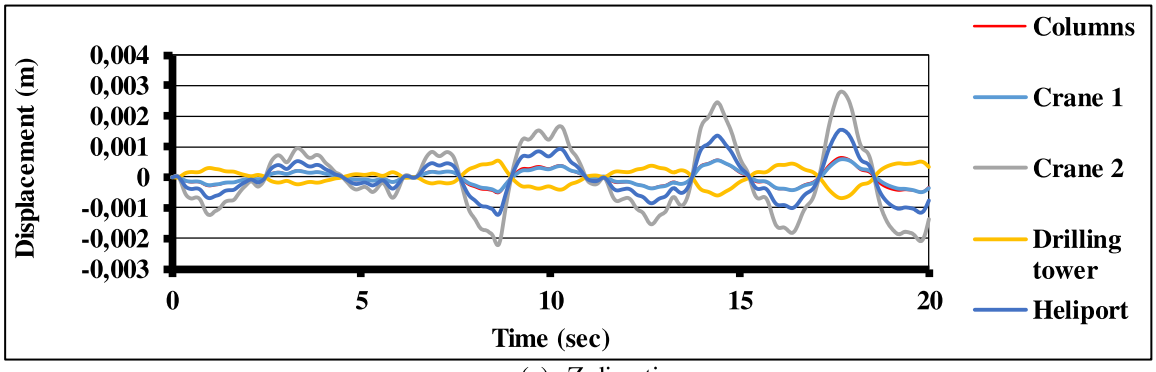

(c) Z-direction

Fig. 18. Displacements of columns and sub-structures during Malaysian earthquake at 70 m hull elevation.

average of the displacements in each level of the columns is calculated. Fig. 14 shows the comparison of the horizontal and vertical displacements of the columns for hull elevation of 70 and 85 m under the El-Centro earthquake. It is obvious that Δ_X is increased by approximately 40 mm or 17% when the hull is in the lowest level (70 m). While the average Δ_Y is increased by approximately 14% when the hull is elevated to the highest level (85 m). Thus, when Δ_X is high, Δ_Y is low for the same model. This non-simultaneous movement for the columns will have a direct effect on the overall structure and may cause its collapse. As expected, Δ_Z is higher when the hull at a higher level, which is raised by approximately 9.5%.

6.1.3. Causes of the Malaysian earthquake excitation

Table 4 shows the displacements of the main three columns during the Malaysian earthquake for both models, four hull corners, top of the two cranes, helicopter port and the top of the drilling tower. The hull corners and the helicopter port are moving simultaneously with the hull, and the displacements are slightly higher. Δ_X for the four corners is increased by approximately 16% when the main hull increases to the highest level. Moreover, Δ_Y for both models is quite similar, but the vertical displacements for the four corners at the highest level are 16% higher than the lowest level. The heliport has about the same percentage of increment in the displacements in both models. However, the two cranes and drilling tower displacements were considered higher than the main hull because of the height of these structures and they are less stiff. The crane displacements in both models have no much difference. Moreover, the displacements for the drilling tower in all directions are increased. Δ_X and Δ_Z are increased by 18.7% and 4%, respectively. However, no much difference in Δ_Y was observed for both models.

For comparison, after calculating the average of the displacements in each level of the columns, two cases of hull elevation under the Malaysian earthquake were compared in terms of horizontal and vertical displacement. Fig. 15 illustrates the hull

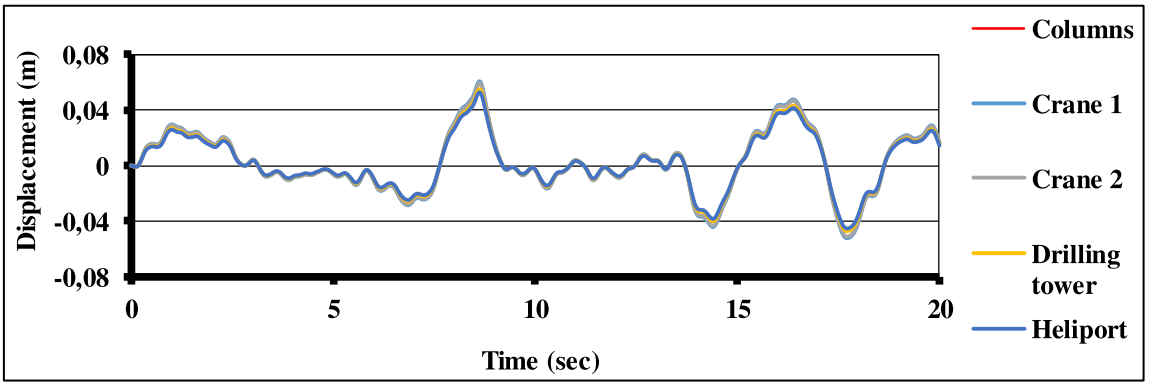

(a) X-direction

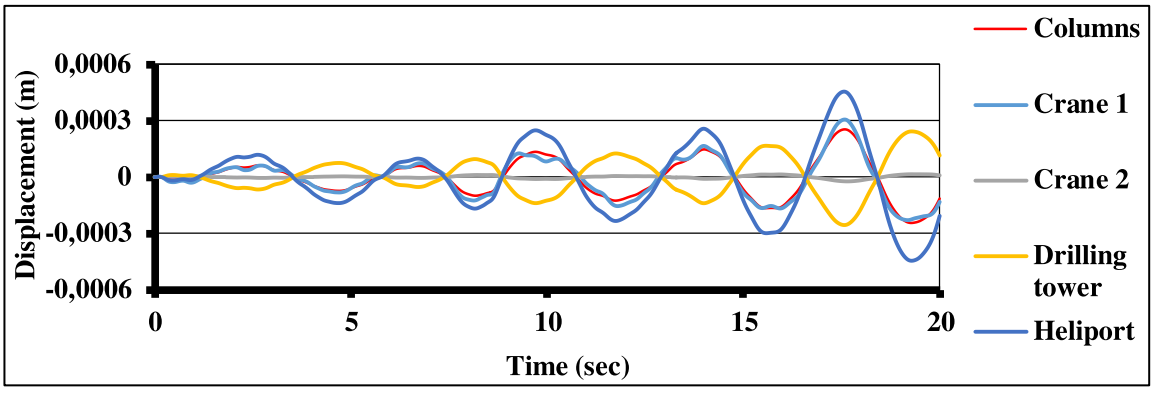

(b) Y-direction

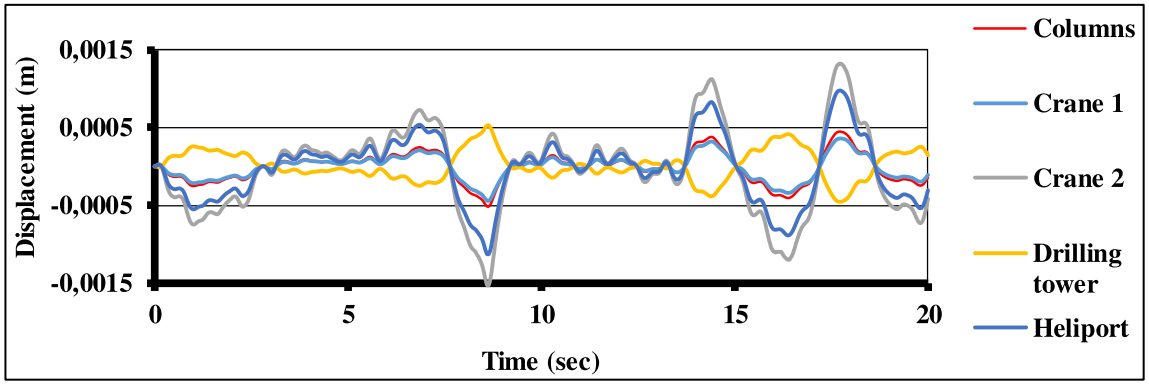

(c) Z-direction

Fig. 19. Displacements of columns and sub-structures during Malaysian earthquake at 85 m hull elevation.

elevations (70 and 80 m) versus displacements under the Malaysian earthquake. The displacements when the hull is in the lowest level are less than those when the hull is higher by approximately 15.2%. Moreover, Δ_Y for both models is quite similar. Furthermore, Δ_Z at a different level are quite similar to those at the ground level until 70 m, but they are 15% higher when the hull is at the highest level.

6.1.4. Causes of tsunami waves at 0°, 45° and 90°

Horizontal and vertical displacements for load combination in two models are compared during tsunami at 0°, 45° and 90° within the lowest and highest hull elevations under the same load combination for hull corners, two cranes, drilling tower and the heliport. Concerning the 0° angle, Table 5 shows the horizontal and vertical displacements for four corners of the hull, top of two cranes, helicopter port and top of drilling tower. That is, the four corners are moving simultaneously with the hull with almost similar displacements in each model. By contrast, Δ_X, Δ_Y and Δ_Z of the four corners are increased in the highest platform deck level by 30%, 32% and 13.3% consecutively. The response of the Jack-up platform structure in the Y-direction under this load combination is small. However, the displacements of the two cranes are considered high in both models compared with those in the main hull because of the height of these structures and they are less stiff. The response of the heliport and drilling tower in vertical and horizontal direction increases when the hull level is increased. However, horizontal Δ_Y for these two sub-structures is very small. At the highest level, Δ_X and Δz of the heliport increased by 30% and 10.5%, respectively. However, the response of the drilling tower in X- and Z-directions is also increased consecutively by approximately 28% and 4.5% with the increase of the hull level.

In terms of the 45° angle, Table 6 shows the displacements during tsunami for hull corners, top of the two cranes, helicopter port and the top of the drilling tower. That is, the hull body and its

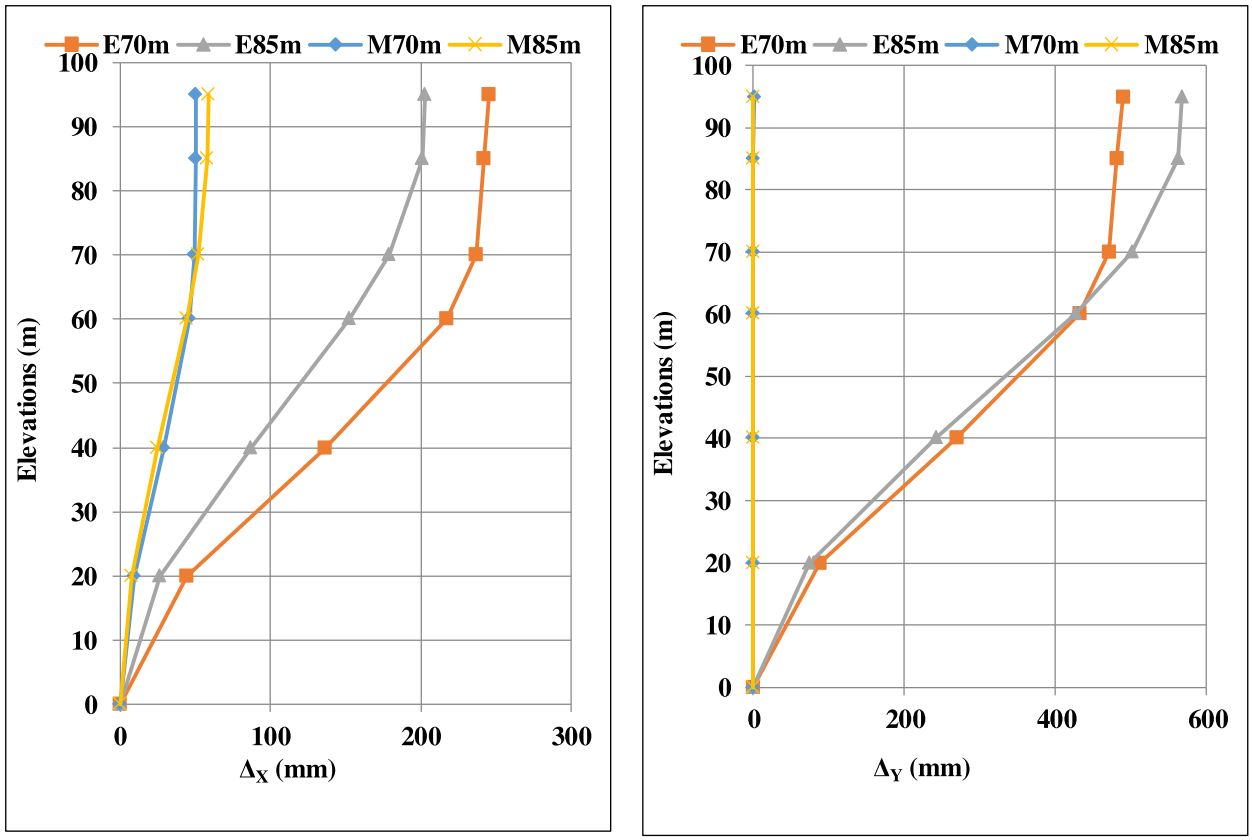

Fig. 20. Horizontal displacements vs. hull elevations due to earthquake excitations.

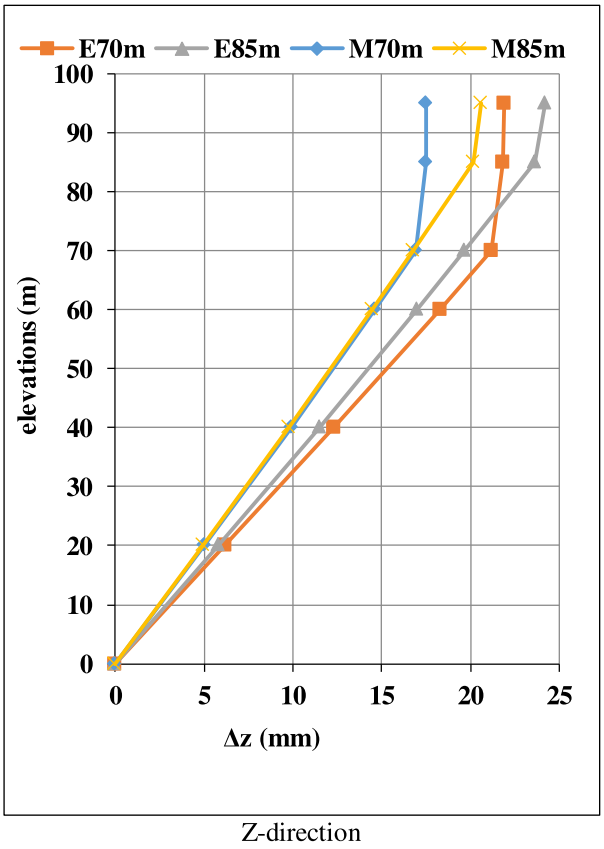

Fig. 21. Vertical displacements vs. hull elevations due to earthquake excitations.

facilities are moving as one element with no much deformation. Horizontal Δ_X and Δ_Y for the four corners, heliport and the drilling tower are increased by approximately 30% and 29% respectively when the platform hull is at the highest level. For the same substructures, the increment in vertical displacement is different. In the jack-up platform, the vertical displacements are increased by 14.5%, 11% and 4% for the four corners, heliport and the drilling tower, respectively. The displacements in vertical and horizontal directions for the two cranes are high.

When at a 90° angle, horizontal and vertical displacements at X-direction within the lowest and highest hull elevations are compared. Table 7 shows the horizontal and vertical displacements for the four corners of the hull, top of the two cranes, helicopter port and the top of the drilling tower. That is, the hull corners, the helicopter port and the drilling tower are moving simultaneously with the hull, and they have almost similar displacements. Corners 1 and 4 of the hull have 45% higher Δ_X than that of the other corners. Moreover, corners 1 and 2 are having higher displacements by 3.6% than the other corners. In terms of the vertical displacement, each corner has Δ_Z that is different from the others. However, horizontal and vertical displacements for the two cranes are considered high compared with the main hull because of the height of these structures and they are less stiff. Moreover, when the hull is at a higher level, the displacements are higher.

6.2. Effect of El-Centro earthquake at the end of columns and sub-structures

6.2.1. Within the lowest hull elevation

Fig. 16 depicts the horizontal and vertical displacements of the columns, two cranes, heliport and drilling column due to the El-

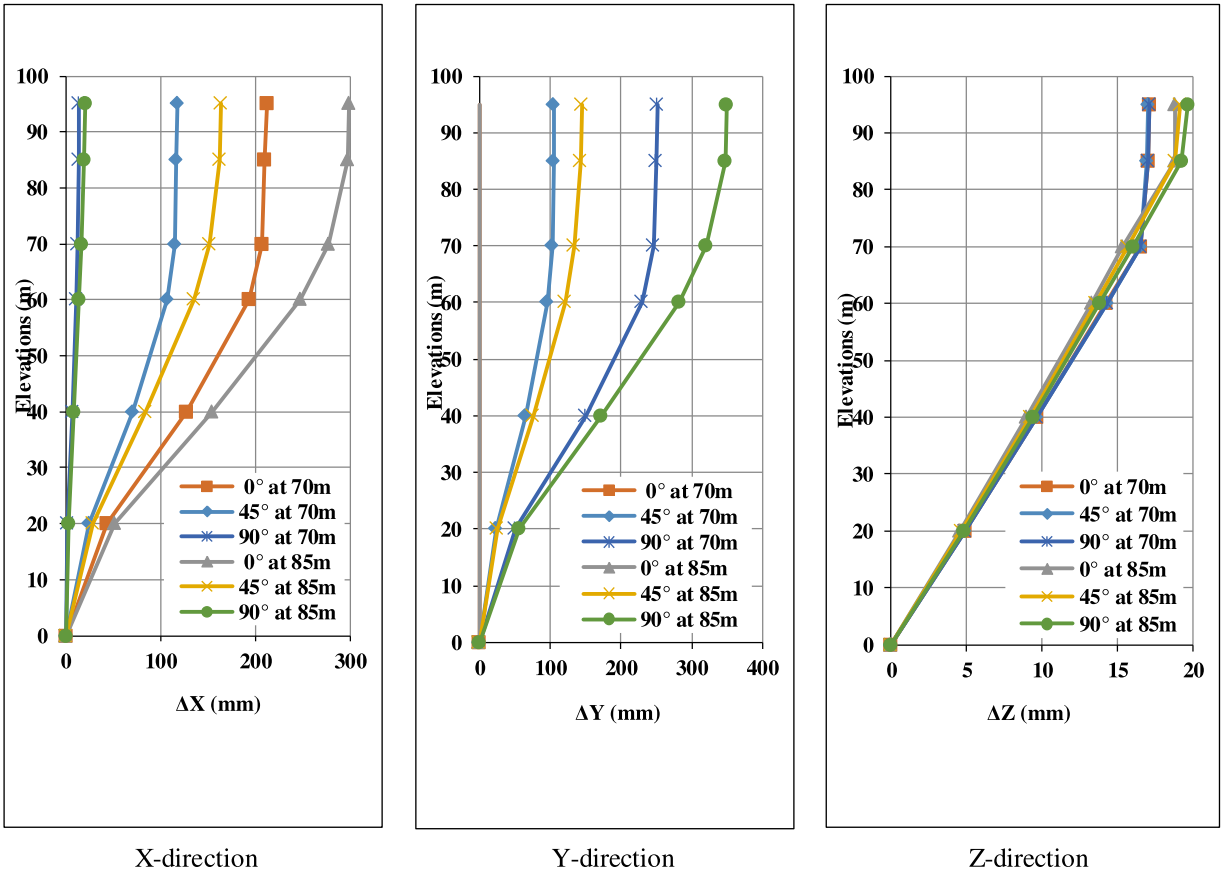

Fig. 22. Displacements vs. hull elevations due to tsunami waves.

Centro earthquake at the lowest hull elevation (70 m). The result shows that the maximum Δ_X, Δ_Y and Δ_Z at the top nodes of the columns and the substructures are 290, 690 and 56 mm, consecutively. In all these cases, the maximum displacement occurred in crane 1.

6.2.2. Within the highest hull elevation

Fig. 17 shows the vertical and horizontal displacements of the columns, two cranes, helicopter pad and drilling column due to the El-Centro earthquake at the highest hull elevation (85 m). The result is interpreted graphically. The results show that the maximum Δ_X at the top nodes is 225 mm, and the maximum Δ_Y at the top nodes of the same elements is 697 mm. Furthermore, the maximum Δ_Z for the same nodes mentioned above is 36 mm, and for the three cases of displacements, the maximum displacements occurred in crane 1.

6.3. Effect of Malaysian earthquake at the end of columns and sub-structures

6.3.1. Within the lowest hull elevation

Horizontal and vertical displacements of columns and substructures due to the Malaysian earthquake in the lowest hull elevation (70 m) are investigated. The results show that the maximum Δ_X, Δ_Y and Δ_Z occurred in crane 1, heliport and crane 2 consecutively, as shown in Fig. 18. These results indicate that the maximum Δ_X, Δ_Y and Δ_Z at the top nodes of columns and substructures are 54, 0.8 and 30 mm respectively.

6.3.2. Within the highest hull elevation

In terms of the highest hull elevation (85 m) due to the Malaysian earthquake, horizontal and vertical displacements of the three columns, two cranes, helicopter pad, and the drilling column are examined. Fig. 19 shows that the maximum horizontal Δ_X at the top nodes of the columns and the substructures is 60.6 mm, which occurred in crane 1. The maximum Δ_Y at the top nodes of the same elements is 0.45 mm, which occurred in the heliport. Furthermore, the maximum Δ_Z for the same nodes mentioned above is 15 mm, which occurred in crane 2.

6.4. Comparison of El-Centro and Malaysian earthquake in terms of horizontal and vertical column displacements

To clarify the results of the two cases of hull elevation under El-Centro and Malaysian earthquake excitations in terms of horizontal and vertical displacements of the three columns, the average displacement in each level of the columns is calculated. Fig. 20 shows the comparison of the 70 and 85 m hull elevation versus the horizontal displacements of the columns under earthquake waves. Δ_X under the El-Centro earthquake is the highest for both models. The effect of the El-Centro earthquake when the hull is at the lowest level is 80% higher than the effect of the Malaysian earthquake in X-direction, whereas such effect is 71% higher when the platform deck elevation is at 85 m. Furthermore, the El-Centro earthquake has the greatest effect on the platform in Y-direction. Thus, the El-Centro earthquake is 99.8% of Δ_Y higher than the Malaysian earthquake in both models.

Fig. 21 shows the comparison of the 70 and 85 m hull elevation and the vertical displacements of the columns under earthquake waves. Δ_Z under the El-Centro earthquake is the highest for both models. The El-Centro earthquake effect increased by 20% compared with the effect of the Malaysian earthquake when the

hull at the lowest elevation. However, the increase in effect is only 14.7% when the platform deck elevation is at the highest level.

Notably, offshore engineers should consider the earthquake effect during designing the offshore platform structures. Given this fact, results show that under the El-Centro earthquake, the horizontal and the vertical displacements for both cases are large, particularly when the hull is at its higher level. Although the hull is in the lowest or highest level, the horizontal and the vertical displacements response is increased during the El-Centro earthquake. However, the percentage of this increment is decreased when the platform deck increases. To conclude, the structure under the Malaysian earthquake is considered safe. However, both models under the El-Centro earthquake are not safe and may collapse or cause major damage.

6.5. Comparison amongst three different cases of tsunami effect in terms of horizontal and vertical displacements

The average displacement in each level of columns is calculated to compare the two models under tsunami waves from different directions in terms of horizontal and vertical displacement. Fig. 22 represents the comparison of the 70 and 85 m hull elevation with the horizontal displacement of the columns under tsunami waves in three different directions about X. Δ_X and Δ_Y of columns have a variety. In the case when the tsunami waves are in the X-direction, Δ_X is the highest in both hull elevations, and Δ_Y is the lowest. However, in the three directions of the tsunami effect, when the hull is in the highest elevation, the displacement is higher. Additionally, Δ_Z in different levels are quite similar from the ground level until 70 m, but they are getting higher in the case when the hull is in the highest level, as shown in Fig. 22.

Horizontal and vertical displacements in both cases are considered high specifically when the hull is at its higher level and depends on the wave direction. The structure under the three cases is considered safe. Furthermore, a big difference in displacements is observed when the hull is in the highest or lowest level. However, the displacements of the cranes and drilling tower are considered high compared with those in the main hull.

7. Conclusion

The current research aims to demonstrate the performance of the jack-up platforms facing a combination of severe dynamic loads (earthquake, tsunami wave and wind forces) using the finite element model for two models with the lowest and highest hull altitudes. High and moderate seismic earthquake accelerations were applied. In addition, tsunami waves were applied to the platform in three different directions, that is, 0°, 45° and 90°, to acquire a variety of displacements. The study selected Airy's linear wave theory to evaluate surface elevations and wave kinematics. Reference wind velocity was specified of 10 knots at commonly 10 m above the mean water level. The results revealed that the combination of the El-Centro earthquake, dead and alive loads, has given the greatest impact on the platform on the lowest and highest hull elevations. Thus, this load combination has more displacements than the other load combinations, such as Malaysian earthquake and tsunami waves. El-Centro earthquake influence has increased by 20% compared with that of the Malaysian earthquake when the hull is at 70 m elevation. On the contrary, the increase is only 14.7% when the platform deck elevation is at 85 m. The horizontal and vertical displacements were increased by 16% and 5.6% when the platform hull increased to the highest level (85 m). By increasing the platform hull elevation, the horizontal and the vertical displacements, due to tsunami loads, have increased by 30% and 15% respectively. Increasing the deck elevation has boosted the response of the dynamic load and displacements but negatively affects the platform. This percentage of the increment in displacements depends on the applying load and the directions.

Cranes and drilling tower are not stable under El-Centro earthquake and tsunami waves because of their relative height. Moreover, the helicopter port is safe under all applying load as it is considered the only way for evacuation during disasters. The hull of the platform has deformed under El-Centro and tsunami loads at 45°, which is at the lowest level of the hull and may affect the serviceability and capability of the platform to withstand the forces. The model of the jack-up platform structure used in this investigation has exceeded the allowable displacements under the El-Centro earthquake and tsunami waves. To protect this structure from collapse, developing a new type of offshore structures by using temporary truss braces with the mechanism of jack-up legs is significant.

Further dynamical studies are required for the jack-up platform to experience more load combinations owing to the importance of this construction in the engineering field, offshore structure and oil industry exploration. The damping system can be applied to resist the dynamic loads of earthquakes and ocean waves although the use of this system is costly. Moreover, future studies may develop a new type of offshore structures to resist these kinds of forces by using temporary truss braces with the mechanism of jack-up legs.

Declaration of competing interest

The authors declare that they have no known competing financial interests or personal relationships that could have appeared to influence the work reported in this paper

References

[1] W. Deng, X. Tian, X. Han, G. Liu, Y. Xie, Z. Li, Topology optimization of jack-up offshore platform leg structure, Proc. Institut. Mech. Eng. Part M 235 (1) (2021) 165–175, doi:10.1177/1475090220928736.
[2] S.K. Chaturvedi, A case study of tsunami detection system and ocean wave imaging mechanism using radar, J. Ocean Eng. Sci. 4 (3) (2019) 203–210, doi:10.1016/j.joes.2019.04.005.
[3] I.S. Abbood, S.a. Odaa, K.F. Hasan, M.A. Jasim, Properties evaluation of fiber reinforced polymers and their constituent materials used in structures – A review, Mater. Today 43 (2) (2020) 1003–1008, doi:10.1016/j.matpr.2020.07.636.
[4] S.S. Weli, I.S. Abbood, K.F. Hasan, M.A. Jasim, Effect of steel fibers on the concrete strength grade: a review, IOP Conf. Ser.: Mater. Sci. Eng. 888 (1) (2020) 012043, doi:10.1088/1757-899x/888/1/012043.
[5] K.S. Ahmed, A.K. Keng, K.C. Ghee, Stress and stiffness analysis of a 7-teeth pinion/rack jacking system of an Offshore jack-up rig, Eng. Fail. Anal. 115 (2020) 104623, doi:10.1016/j.engfailanal.2020.104623.
[6] S.F. Leijten, M. Efthymiou, A philosophy for the integrity assessment of jackup units, SPE Drill. Eng. 6 (02) (1991) 125–130, doi:10.2118/19236-PA.
[7] Z. Tian, F. Liu, L. Zhou, C. Yuan, Fluid-structure interaction analysis of offshore structures based on separation of transferred responses, Ocean Eng. 195 (2020) 106598, doi:10.1016/j.oceaneng.2019.106598.
[8] X. Bai, A. Guo, H. Liu, W. Chen, G. Liu, T. Liu, S. Chen, H. Li, Experimental investigation on a freestanding bridge tower under wind and wave loads, Struct. Eng. Mech. 57 (5) (2016) 951–968, doi:10.12989/sem.2016.57.5.951.
[9] N. Flores-Guzmán, E. Olivera-Villaseñor, A. Kryvko, A. Rodríguez-Castellanos, F. Sánchez-Sesma, Seismic pressures in offshore areas: Numerical results, Latin Am. J. Solid. Struct. 13 (16) (2016) 3062–3084, doi:10.1590/1679-78252376.
[10] S. Tuty, M.J. Cassidy, B.F. Ronalds, Investigation of shallow water kinematics and local loading effects on reliability of minimum structures, J. Offshore Mech. Arctic Eng. 124 (1) (2002) 41–47, doi:10.1115/1.1423910.
[11] R. Lubeena, V. Gupta, Wave loading on offshore structures, Offshore Technology Conference, Houston, Texas, USA, 2013 https://doi.org/10.4043/24146-MS.
[12] API, in: API Recommended Practice 2A-WSD: Planning, Designing, and Constructing Fixed Offshore Platforms - Working Stress Design, 22nd Edition, American Petroleum Institute, Washington, DC, USA, 2014, p. 310.
[13] K.A. Digre, F. Zwerneman, Insights Into Using the 22nd Edition of API RP 2A Recommended Practice For Planning, Designing and Constructing Fixed Offshore Platforms - Working Stress Design, in: Insights Into Using the 22nd Edition of API RP 2A Recommended Practice For Planning, Designing and Constructing Fixed Offshore Platforms - Working Stress Design, Offshore Technology Conference, Houston, Texas, USA, 2012.
[14] B. He, S. Hou, X. He, J. Nie, Virtual prototyping-based integrated information modeling and its application in the jacking system of offshore platform, Int. J. Hybrid Inf. Technol. 6 (6) (2013) 135–148, doi:10.14257/ijhit.2013.6.6.12.

[15] N. Abdussamie, G. Thomas, W. Amin, R. Ojeda, Wave-in-deck forces on fixed horizontal decks of offshore platforms, ASME, San Francisco, California, USA, 2014 https://doi.org/10.1115/OMAE2014-23629.
[16] B. Buchner, T. Bunnik, Extreme wave effects on Deepwater floating structures, Houston, Texas, USA, 2007 https://doi.org/10.4043/18493-MS.
[17] S.K. Chaturvedi, P.K. Srivastava, U. Guven, A brief review on tsunami early warning detection using BPR approach and post analysis by SAR satellite dataset, J. Ocean Eng. Sci. 2 (2) (2017) 83–89, doi:10.1016/j.joes.2016.12.001.
[18] S.K. Chaturvedi, U. Guven, P.K. Srivastava, Measurement and validation of tsunami Eigen values for the various water wave conditions, J. Ocean Eng. Sci. 5 (1) (2020) 41–54, doi:10.1016/j.joes.2019.08.001.
[19] T. Shibayama, M. Esteban, I. Nistor, H. Takagi, N.D. Thao, R. Matsumaru, T. Mikami, R. Aranguiz, R. Jayaratne, K. Ohira, Classification of tsunami and evacuation areas, Natural Hazards 67 (2) (2013) 365–386, doi:10.1007/s11069-013-0567-4.
[20] R. Jayaratne, T. Mikami, M. Esteban, T. Shibayama, Investigation of Coastal Structure Failures due to the 2011 Great Eastern Japan Earthquake Tsunami, in: From Sea to Shore – Meeting the Challenges of the Sea, ICE Publishing, 2014, pp. 1241–1250.
[21] Guidelines for design of structures for vertical evacuation from tsunamis, 3rd Edition, Applied Technology Council, California, USA, 2019.
[22] G.T. Houlsby, A.M. Puzrin, in: The bearing capacity of a strip footing on clay under combined loading, Royal Society, London, 1999, pp. 893–916. https://doi.org/10.1098/rspa.1999.0340.
[23] M.J. Jun, Y.H. Kim, M.S. Hossain, M.J. Cassidy, Y. Hu, S.G. Park, Global jack-up rig behaviour next to a footprint, Marine Struct. 64 (2019) 421–441, doi:10.1016/j.marstruc.2018.12.002.
[24] S. Guo, H. Zhuang, W.-x. Tang, W.-l. Wu, Q. Liu, Y.-y. Wang, Design of a bionic spudcan and analysis of penetration and extraction performances for jack-up platform, China Ocean Eng. 34 (1) (2020) 80–88, doi:10.1007/s13344-020-0008-6.
[25] A.R. Chaudhry, Static pile-soil-pile interaction in offshore pile groups, University of Oxford, UK, 1994 https://ethos.bl.uk/OrderDetails.do?uin=uk.bl.ethos.260751.
[26] I.S. Abbood, S.S. Weli, F.L. Hamid, Cement-based materials for self-sensing and structural damage advance warning alert by electrical resistivity, Mater. Today (2021), doi:10.1016/j.matpr.2020.11.381.
[27] M.J. Cassidy, P.H. Taylor, R.Eatock Taylor, G.T. Houlsby, Evaluation of long-term extreme response statistics of jack-up platforms, Ocean Eng. 29 (13) (2002) 1603–1631, doi:10.1016/S0029-8018(01)00110-X.
[28] G. Li, D.-y. Zhang, Q.-J. Yue, Minimum life-cycle cost design of ice-resistant offshore platforms, Struct. Eng. Mech. 31 (1) (2009) 11–24, doi:10.12989/sem.2009.31.1.011.
[29] G. Liu, Y. Sun, B. Zhong, Y. Xie, A. Incecik, Z. Li, Analysis of wind load effect on key components in a jack-up offshore platform, Appl. Ocean Res. 101 (2020) 102263, doi:10.1016/j.apor.2020.102263.
[30] G. Barbaro, B. Ierino, M.C. Martino, in: Maximum force produced by wind generated waves on offshore maritime structures, ASME, San Diego, California, USA, 2007, pp. 651–658. https://doi.org/10.1115/OMAE2007-29534.
[31] R. Zakhama, M.M. Abdalla, Z. Gürdal, H. Smaoui, Wind load effect in topology optimization problems, J. Phys. 75 (2007) 012048, doi:10.1088/1742-6596/75/1/012048.
[32] Y. Zhao, Z. Cheng, P.C. Sandvik, Z. Gao, T. Moan, E. Van Buren, Numerical modeling and analysis of the dynamic motion response of an offshore wind turbine blade during installation by a jack-up crane vessel, Ocean Eng. 165 (2018) 353–364, doi:10.1016/j.oceaneng.2018.07.049.
[33] K. Bargi, S.R. Hosseini, M.H. Tadayon, H. Sharifian, Seismic response of a typical fixed jacket-type offshore platform (SPD1) under sea waves, Open J. Marine Sci. 1 (2) (2011) 36–42, doi:10.4236/ojms.2011.12004.
[34] D.-.H. Park, J.-.H. Kim, Y.-J. Park, J.-.H. Jeon, M.-.H. Kim, J.-.M. Lee, Parametric study for suggestion of the design procedure for offshore plant helideck subjected to impact load, Struct. Eng. Mech. 60 (5) (2016) 851–873, doi:10.12989/sem.2016.60.5.851.
[35] Q. Yin, J. Yang, G. Xu, R. Xie, M. Tyagi, L. Li, X. Zhou, N. Hu, G. Tong, C. Fu, D. Pang, Field experimental investigation of punch-through for different operational conditions during the jack-up rig spudcan penetration in sand overlying clay, J. Petrol. Sci. Eng. 195 (2020) 107823, doi:10.1016/j.petrol.2020.107823.
[36] X.M. Tang, J. Li, C. Lu, Q.H. Cheng, Numerical analysis of jacking operations for a self-elevated jack-up unit, Eng. Comp. 19 (2) (2003) 152–159, doi:10.1007/s00366-003-0254-2.